agronomy

MDPI

Article

Influence of Hydroxyapatite Nanoparticles on Germination and Plant Metabolism of Tomato (*Solanum lycopersicum* L.): Preliminary Evidence

Luca Marchiol [1,*], Antonio Filippi [1], Alessio Adamiano [2], Lorenzo Degli Esposti [2,3], Michele Iafisco [2], Alessandro Mattiello [1], Elisa Petrussa [1] and Enrico Braidot [1]

1 Department of Agri-Food, Animal and Environmental Sciences, University of Udine, via delle Scienze 206, 33100 Udine, Italy; antoniofilippi@yahoo.it (A.F.); alessandro.mattiello@uniud.it (A.M.); elisa.petrussa@uniud.it (E.P.); enrico.braidot@uniud.it (E.B.)

2 Institute of Science and Technology for Ceramics (ISTEC), National Research Council (CNR), Via Granarolo 64, 48018 Faenza (RA), Italy; alessio.adamiano@istec.cnr.it (A.A.); lorenzo.degliesposti@istec.cnr.it (L.D.E.); michele.iafisco@istec.cnr.it (M.I.)

3 Department of Chemistry, Life Sciences and Environmental Sustainability, University of Parma, Parco Area delle Scienze 17/a, 43124 Parma, Italy

* Correspondence: luca.marchiol@uniud.it; Tel.: +39-432-558611

Received: 28 February 2019; Accepted: 23 March 2019; Published: 27 March 2019

Abstract: The Nutrient Use Efficiency in intensive agriculture is lower than 50% for macronutrients. This feature results in unsustainable financial and environmental costs. Nanofertilizers are a promising application of nanotechnology in agriculture. The use of nanofertilizers in an efficient and safe manner calls for knowledge about the actual effects of nanoproducts on the plant metabolism and eventually on the carrier release kinetics and nutrient accumulation. Hydroxyapatite ($Ca_{10}(PO_4)_6(OH)_2$) nanoparticles (*n*HA) have an interesting potential to be used as nanofertilizers. In this study, the effects of different *n*HA solutions stabilized with carboxymethylcellulose (CMC) were evaluated on germination, seedling growth, and metabolism of *Solanum lycopersicum* L., used as model species. Our observations showed that the percentage germination of *S. lycopersicum* is not influenced by increasing concentrations of *n*Ha, while root elongation is strongly stimulated. Tomato plants grown in hydroponics in the presence of *n*HA have not suffered phytotoxic effects. We conclude that *n*HA had nontoxic effects on our model plant and therefore it could be used both as a P supplier and carrier of other elements and molecules.

Keywords: phyto-nanotechnology; nanofertilizers; hydroxyapatite nanoparticles

1. Introduction

The current agriculture model is based on a progressive expansion of arable lands and increased input of energy, fertilizers, pesticides, and water [1]. The Nutrient Use Efficiency (NUE) is the relationship between the amount of nutrients acquired by plants and the resulting production of biomass [2]. Due to soil physicochemical properties, and to the characteristics of most used fertilizers, the NUE for macronutrients in crops is lower than 50%. For this reason, the intensive cultivation of crops has unsustainable financial and environmental costs [3].

Nanotechnologies allow the control and manipulation of matter on an atomic and molecular scale. The novel physicochemical properties of nanomaterials, i.e., catalytic reactivity, high surface area, size, and shape, have the potential to solve the problems in primary production and maximizes productivity in agriculture [4].

The application of nanotechnology in the plant production systems has been defined as "phyto-nanotechnology" [5]. One of the most promising applications of phyto-nanotechnology concerns crop fertilization. The term "nanofertilizer" refers to a structure in the dimension of 1–100 nm that delivers macro/micronutrients to crops. In addition, this term should also be extended to indicate bulk materials used together with nanoscale structures to construct new products [6]. Conventional fertilizers have low nutrient uptake efficiencies and are often associated with high losses to the environment. Therefore, the key-point of modern crop fertilization is to avoid these nutrient losses and synchronize the nutrient availability with its uptake by crops [7,8]. However, the extremely appealing prospects of nanofertilizers in large part have still to be experimentally demonstrated in field conditions [9–11].

With regard to plant macronutrients, studies on hydroxyapatite ($Ca_{10}(PO_4)_6(OH)_2$) nanoparticles (*n*HA) explored their potential use as carrier of nitrogen (N) or as phosphorus (P) fertilizer. The main advantage of using *n*HA with respect to other nanomaterials is that they are widely renowned for their intrinsic biocompatibility and biodegradability, being the main component of human bones and teeth [12–14]. Thus, when considering open field application of nanoparticles, the safe biologic profile of *n*HA should not raise any concern on human and environmental health.

A very early study concerning the use of *n*HA as N carrier through their coupling with urea (U) was provided by Kottegoda et al. and demonstrated a significant slower release of N by the nanohybrid structure than the conventional U [15]. In another study, the effects of conventional U and U-*n*HA on seed germination and seedling growth of *Vigna radiata* were compared. The nanohybrid gave the better results, increasing the germination rate and the biomass yield [16]. The N agronomic use efficiency in plants of *Oryza sativa* supplied with U-*n*HA and conventional U was compared. The expected slower N release by HA-U resulted in a better N-efficiency compared to traditional fertilizer [17].

Some other studies investigated structures of higher complexity involving *n*HA. In particular, the fertilizing potential of the nanocomposites Urea-Hydroxyapatite-Montmorillonite (U-*n*HA-MMT) and U-*n*HA encapsulated wood chips were tested on *Festuca arundinacea*. It was demonstrated that both nanocomposites decreased N leaching and caused a slower N release compared to conventional fertilizers [18]. More recently, a life cycle study on *Oryza sativa* supplied with U-*n*HA-MMT was carried out. A significant decrease of N release from soil columns and the crop yield enhancement were recorded [19]. To the best of our knowledge, only two papers reported data regarding the use of *n*HA as P fertilizer on *Glycine max* [20] and *Triticum aestivum* [21], separately. The experimental results demonstrated that root and aerial plant biomass were enhanced respectively by 41% and 18.2% with respect to the conventional P fertilizer.

In order to use nanofertilizers efficiently, accurate knowledge of carrier release kinetics is required. At the same time, it is also necessary to know what are the effects produced by the carriers themselves on the plants. In this regard, no systematic studies concerning the effects of *n*HA on plants have been carried out, so far. In this study, the effects of different concentrations of *n*HA stabilized with carboxymethylcellulose (CMC) were evaluated on germination, seedling growth, and metabolism of *Solanum lycopersicum* L., used as a model plant.

2. Materials and Methods

2.1. Hydroxyapatite Nanoparticles Preparation

Calcium acetate ($Ca(CH_3COO)_2$, 99.0% pure), phosphoric acid (H_3PO_4, 85.0% pure), aqueous ammonia (NH_4OH, 28.0% pure), carboxymethylcellulose (low density, M.W. $\approx$ 90 kDa), and bulk hydroxyapatite (bHA) were purchased from Sigma Aldrich (St. Luis, MO, USA) and used without further purification. All the solutions were prepared with ultrapure water (18.2 MΩ $\times$ cm, 25 °C, arium© pro, Sartorius, Goettingen, Germany).

HA nanoparticles were prepared as reported by Sandhofer et al. [22]. Briefly, nanoparticles were synthesized at room temperature by dropping a solution of H_3PO_4 (0.21 M) into a solution of

$Ca(CH_3COO)_2$ (0.35 M) maintaining the pH at a constant value of 10 by the addition of NH_4OH. The reaction mixture was kept under stirring at room temperature overnight; then the stirring was suspended and the mixture was left standing still for 2 h. The reaction mixture was finally centrifuged at 6000 rpm for 7 min and the obtained pellet was repeatedly washed and suspended in ultrapure water up to 10,000 mg L^{-1}.

*n*HA was stabilized with CMC according to Liu et al. [20]. Briefly, 5 g of suspended *n*HA at 10,000 mg L^{-1} was sonicated for 30 min, before adding 5 g of CMC. The mixture was then kept under vigorous stirring at room temperature overnight. The solutions used for plant experiments were prepared by diluting CMC stabilized *n*HA suspension with CMC 1% (w/v) aqueous solution for seed germination experiments, and with CMC 1% (w/v) full strength Hoagland solution for seedling hydroponic culture experiments.

2.2. Hydroxyapatite Chemical, Morphological, and Structural Characterization

X-ray diffraction (XRD) patterns of the powder samples were recorded on a D8 Advance diffractometer (Bruker, Karlsruhe, Germany) equipped with a Lynx-eye position sensitive detector using Cu Kα radiation (λ = 1.54178 Å) generated at 40 kV and 40 mA. Spectra were recorded in the 2θ range from 10° to 60° with a step size (2θ) of 0.02 and a counting time of 0.5 s.

The average size of crystal domains along the apatite axis directions ($D_{(002)}$) and ($D_{(310)}$) was calculated by applying Scherrer's equation:

$$D_{[hkl]} = \frac{0.9\lambda}{cos\theta\sqrt{(\Delta_r^2) - (\Delta_0^2)}}$$

where θ is the diffraction angle for plane (hkl), Δ_r and Δ_0 are the widths in radians of the reflection (hkl) at half height for the synthesized and pure inorganic hydroxyapatite (standard reference material, calcium hydroxyapatite, National Institute of Standards & Technology), respectively, and λ = 1.5405 Å. The PXRD patterns were background corrected before the Scherrer's analysis.

Fourier transform infrared (FT-IR) spectroscopy analyses were carried out on a Nicolet iS5 spectrometer (Thermo Fisher Scientific Inc., Waltham, MA, USA) with a resolution of 2 cm^{-1} by accumulation of 64 scans covering the 4000 to 400 cm^{-1} range, using a diamond ATR accessory model iD7.

Sample morphology and size in dry state were analyzed with a FEI Tecnai F20 transmission electron microscopy (TEM) equipped with a Schottky emitter and operating at 120 and 200 keV. Ten µL of *n*HA suspension in ultrapure water at 10.0 mg mL^{-1} were dissolved in 5 mL of isopropanol and treated with ultrasound. A droplet of the resulting finely dispersed suspensions was evaporated at room temperature and under atmospheric pressure over night on a holey carbon film supported on a copper grid.

Quantification of Ca and P was carried out by ICP-OES (Agilent Technologies 5100 ICP-OES, Santa Clara, CA, USA). Samples were prepared dissolving an aliquot of freeze-dried *n*HA powder in a 1% (w/v) HNO_3 solution.

Thermogravimetry analyses (TGA) were performed using a STA 449F3 Jupiter (Netzsch GmbH, Selb, Germany) apparatus. About 10 mg of freeze-dried *n*HA powder was weighted in an alumina crucible and heated from room temperature to 1100 °C under air flow with a heating rate of 10 °C/min. The weight losses were attributed to (i) adsorbed and structural water for the temperature range from room temperature to 200 °C, (ii) residual acetate for the temperature range from 200 to 600 °C, and (iii) carbonate for the temperature range 600 to 1000 °C.

Size distribution of *n*HA samples were evaluated by dynamic light scattering (DLS). CMC stabilized *n*HA were suspended in Hoagland full strength solution with CMC 1% (w/v); the so obtained suspension was analyzed by DLS using a Zetasizer Nano Series (Malvern, UK) by backscatter detection (λ = 630 nm, θ = 173°). Particle size (reported as Z-average) was reported as the average

and the standard deviation of three measurements of 10 runs for 10 s at 25 °C. The viscosity and the refractive index of the Hoagland solution containing 1% (w/v) of CMC were 7 cP and 1.33, respectively.

2.3. Plant Experiment

2.3.1. Treatments

The treatment solutions were prepared by sequential dilutions from a *n*HA stock solution of 10,000 mg mL^{-1} with the addition of 1% (w/v) CMC. The CMC-*n*HA solution at 10,000 mg mL^{-1} was sonicated for 30 min in order to avoid the nanoparticles aggregation. Then it was sequentially diluted with a solution of CMC 1% in deionized water to obtain the treatment solutions used for plant experiments. The CMC solution at 1% (w/v) represented the control. The same procedure was used to prepare the bulk hydroxyapatite (bHA).

2.3.2. Seed Germination and Root Elongation

Seeds of tomato (*Solanum lycopersicum* L. cv. Marglobe) were soaked in each treatment solution for 12 h. Thirty seeds were placed in sterile Petri dishes (96 mm diameter × 16 mm height) on filter paper moistened with about 4 mL of deionized water (control) and treatment solution (2, 20, 200, 500, 1000, and 2000 mg L^{-1}). Petri dishes were wrapped with an aluminum foil and incubated at 21 ± 2 °C and 10/14 h light/dark. After 9 days, the germinated seeds were counted. The seeds were considered germinated when the length of the primary root was equal or more than 2 mm. The length of primary roots was measured by using ImageJ (1.48 r).

2.3.3. Seedling Hydroponic Culture

Nine-day-old tomato seedlings were transferred in an aerated hydroponic system in controlled conditions (21 ± 2 °C and 10/14 h light/dark) and supplied by a half strength Hoagland nutrient solution. After 7 days, the nutrient solution was adjusted to full strength Hoagland for 2 weeks. At fully expanded third leaf, the seedlings were treated with 0, 20, 200, 500, and 2000 mg L^{-1} of CMC-*n*HA and 2000 mg L^{-1} of bHA solutions for 48 h. Each treatment had six replicates.

2.3.4. ICP-MS Analysis

At harvest, plant biomass was divided into roots and shoots (stems and leaves). The plant fractions were then oven-dried for 24 h at 105 °C. Samples of root and shoot material were digested in 5 mL of a 1 to 4 (v/v) mixture of 37% (v/v) HCl and 65% (v/v) HNO_3 in Teflon cylinders for 10 min at 180 °C in a microwave oven (CEM, Mars Xpress). Then the sample volume was adjusted to 20 mL with milli-Q water and filtrated through 0.45 µm Teflon filters. Ca and P concentrations were determined by an ICP-MS (NexIon 350, Perkin Elmer, Waltham, MA, USA). The accuracy of the analytical procedure was checked by running a certified reference material (NIST SRM® 1573 tomato leaves) every 10 samples.

2.3.5. Reactive Oxygen Species (ROS) Determination

The generation of ROS was monitored according to the method used by Filippi et al. [23]. Root and shoot samples of tomato were ground with liquid nitrogen and 100 mg of the obtained powder was resuspended in 50 mM Tris-HCl (pH 7.5), centrifuged at 10,000× g and the supernatant was used for the assay.

2.3.6. Photosynthetic Pigments Quantification

Photosynthetic pigments were quantified according to Mobin and Khan [24] with minor changes: 20 mg of frozen powder obtained from tomato shoot portions ground to powder by liquid nitrogen was mixed with 0.5 mL of cold 90% (v/v) acetone with 0.01 N ammonium hydroxide and then with

0.5 mL of cold 80% (v/v) acetone. After 14,000× *g* centrifugation for 10 min, the supernatant was collected and used for the analysis of pigments, which was carried out by spectrophotometric analysis.

2.3.7. Determination of Cellular ATP

Root and shoot portions were weighted (100 ± 20 mg DW) and frozen by liquid nitrogen. A fine powder was obtained by grinding and it was used for cellular ATP measurement, according to Mattiello et al. [25]. Aliquots (20 or 2 µL, respectively) of root and shoot soluble fraction were added to the incubation mixture. The ATP calibration curve was performed for each experiment and the sample concentrations were then calculated by interpolation.

2.3.8. Data Analysis

All the experiments were carried out with at least three biological replicates, unless differently stated. The results for each parameter were firstly analyzed by descriptive analysis in order to understand the proper statistical inference to apply. The statistical significance of the treatments was evaluated by one-way Analysis of Variance (ANOVA). Means were compared by Least Significant Difference (LSD), according to Fisher's statistical test, where different letters assigned to means designate a statistical difference at $p \leq 0.05$. The ICP data were investigated through non-parametric statistics on the basis of results obtained by descriptive analysis; the means were compared by the Kruskal-Wallis test and when this test highlighted significant differences, the post-hoc analysis was applied through the Mann-Whitney (MWW) pairwise test. Differences in *Z*-average size were analyzed for their statistical significance by two-tailed Student's t-test with $p \leq 0.05$.

3. Results

3.1. nHA and CMC-nHA Characterization

HA nanoparticles (*n*HA) were prepared at room temperature by an acid–base neutralization reaction. The powder X-ray diffraction (PXRD) pattern features weak and broad reflections characteristic of a poorly crystalline hydroxyapatite (Figure 1).

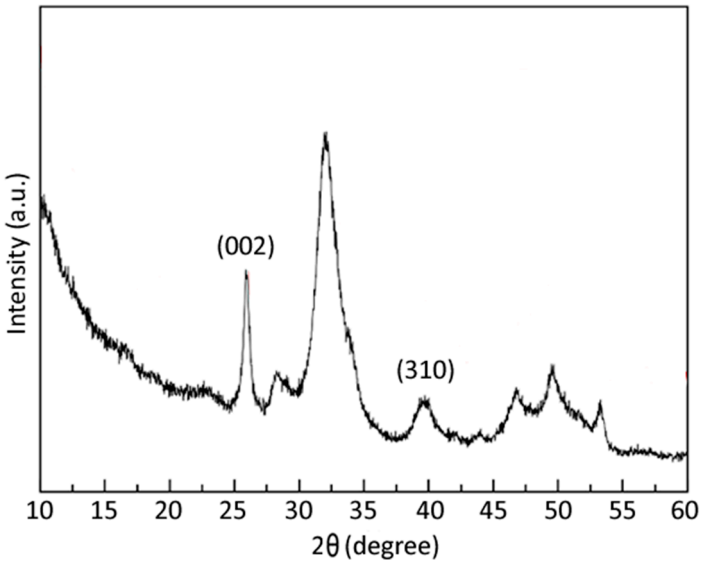

Figure 1. Powder X-ray diffraction (PXRD) pattern of nanoparticles (*n*HA) in the 2θ range from 10° to 60°.

The relative mean domain sizes and the chemical composition (Table 1) are typical of a nanometric, Ca-deficient, and carbonated hydroxyapatite. The domain sizes calculated from the (310) and (002) planes applying Scherrer's formula, representative of nanocrystals *ab* plane and *c* axis, respectively,

evidenced that the nanoparticles are elongated along the *c*-axis, with an aspect ratio (D(002)/D(310)) ≈ 4.5. The Ca/P ratio of *n*HA is 1.60 ± 0.06, which is typical of a poorly crystalline and Ca-deficient hydroxyapatite. A small amount of carbonate ions (≈ 1% w/v) derived from the atmospheric CO_2 adsorbed on the surface and/or entrapped in the lattice of the material during synthesis was detected by thermal gravimetric analysis (TGA). Additionally, a small amount of acetate that remained entrapped on the surface of the HA was calculated by TGA analysis, and corresponded to 1.40 ± 0.1% (w/v).

Table 1. Domain size as measured by PXRD [(a)] and chemical composition of *n*HA as determined by ICP-OES [(b)] and thermal gravimetric analysis (TGA) [(c)].

Sample	D(002) [(a)]	D(310) [(a)]	Ca [(b)]	P [(b)]	Ca/P [(b)]	Carbonate [(c)]
	Size (nm)	Size (nm)	w (%)	w (%)	(mol)	w (%)
*n*HA	16.5	3.6	31.6 ± 1.5	15.2 ± 0.3	1.60 ± 0.06	0.68 ± 0.07

TEM analysis revealed that the *n*HA sample is composed of irregularly shaped plate-like particles often agglomerated and with the major axis ranging between 35 and 45 nm (Figure 2). These results are in good agreement with the crystallite size and the shape factor estimated from the XRD analysis. The aggregation observed in the TEM picture is due to the prevalence of the electrostatic interactions of the nanoparticles surface in the dry state, thus it is not fully representative of the actual nanoparticles condition in aqueous dispersion, nor in the CMC solution.

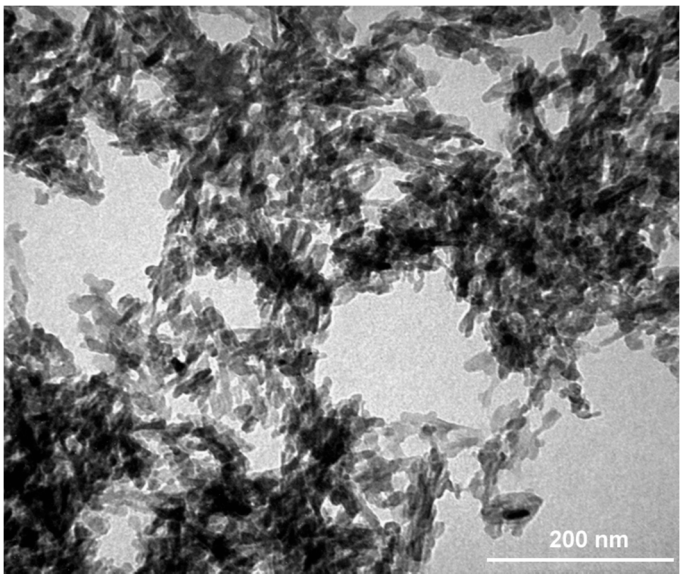

Figure 2. Transmission electron microscopy (TEM) image of *n*HA.

As previously described, *n*HA solution at 10,000 mg L^{-1} was diluted to the concentration of 2, 20, 200, 500, 1000, and 2000 mg L^{-1} before being used on plants. In order to assess the degree of aggregation of nanoparticles in hydroponic experiments, the colloidal properties of *n*HA dispersed in Hoagland full strength and CMC 1 % (w/v) were measured by DLS.

The size distribution of nanoparticles at such concentrations was measured at several time points up to 48 hours (Figure 3). The Z-average of the nanoparticles remained unchanged along all the time points for all the concentrations tested, and corresponded to 94.0 ± 1.3 nm, 96.4 ± 1.0 nm, 109.0 ± 4.2 nm, and 163.3 ± 25.7 nm for the solutions at 2000 mg L^{-1}, 200 mg L^{-1}, 20 mg L^{-1}, and 2 mg L^{-1}, respectively. The same trend was observed for the suspensions used for seed germination experiments up to 10 days, thus confirming the good colloidal stability of *n*HA in the presence of CMC. The error associated with the measured Z-average of the latter samples was found to increase because of the low intensity of the scattered light measured at 20 and 2 mg L^{-1}.

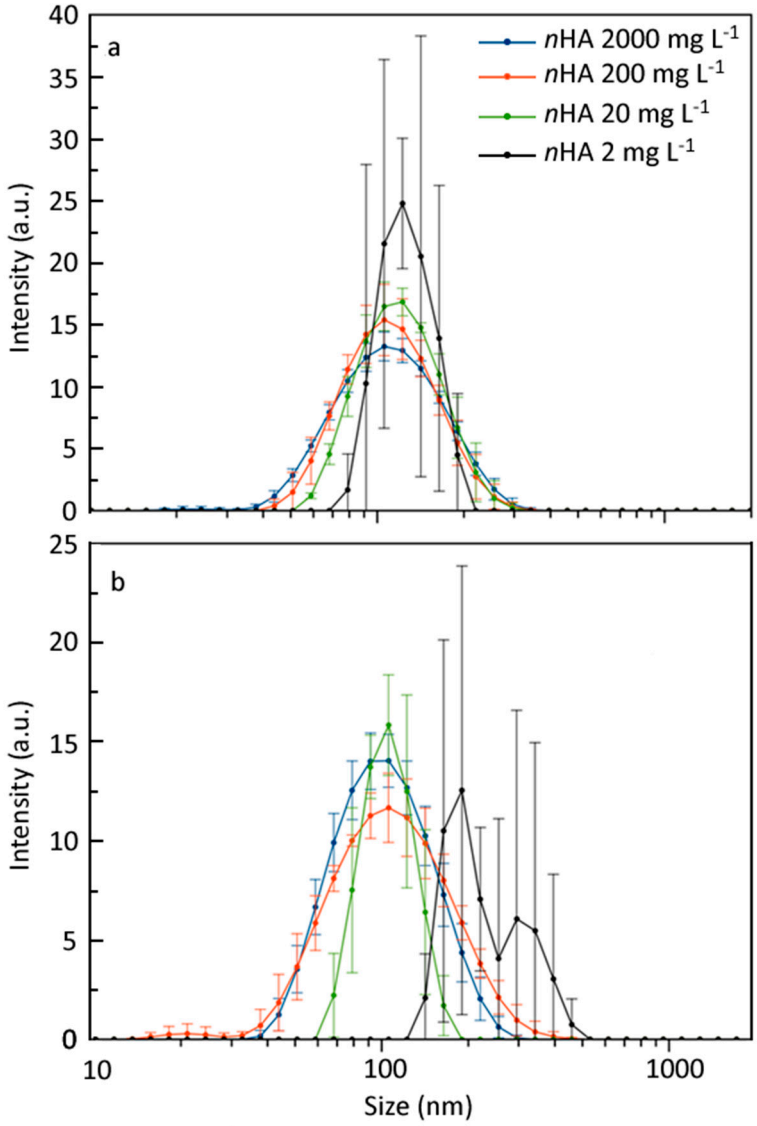

Figure 3. Size distribution measured by dynamic light scattering (DLS) on *n*HA suspension in Hoagland full strenght and carboxymethylcellulose (CMC) 1 % (w/v) at different concentrations after (**a**) 30 min and (**b**) 48 h. Values are expressed as the average of three replicates and error bars represent the relative standard deviation for each size point.

However, all the suspensions displayed a good colloidal stability as no variation nor sedimentation of the nanoparticles was observed for any of the concentrations and conditions tested, with the exception of the suspension at 2 mg L^{-1}. At this latter concentration, an apparent increase of the size at 48 h was noted; however, this was probably an artifact deriving from the very low intensity of the signals recorded by the instrument at this concentration, as can be noted by the very high error associated with the measurements. DLS, in fact, is known to have low resolution, especially in the case of diluted solutions of materials having a low refraction index like hydroxyapatite [Caputo, 2019 #10].

FT-IR spectra of *n*HA (Figure 4) showed the characteristic vibration bands of hydroxyapatite, such as the apatitic PO_4^{3-} vibration bands at 560–603 (ν_4), 962 (ν_1), 1000–1104 cm^{-1} (ν_3), and the apatitic OH^- vibration band at 632 cm^{-1} (ν_LOH, libration mode). *n*HA exhibited also FT-IR bands at 870 (ν_2) and 1420 cm^{-1} (ν_3) assignable to CO_3^{2-} vibrations characteristic of B-type carbonate–apatite (i.e., CO_3^{2-} replacing PO_4^{3-}), confirming the partial carbonate replacement of phosphate observed in the chemical analyses. The presence of a small amount of acetate ions entrapped on the surface of HA was revealed by a weak band at ca. 1600 cm^{-1} (ν_{as}OCO).

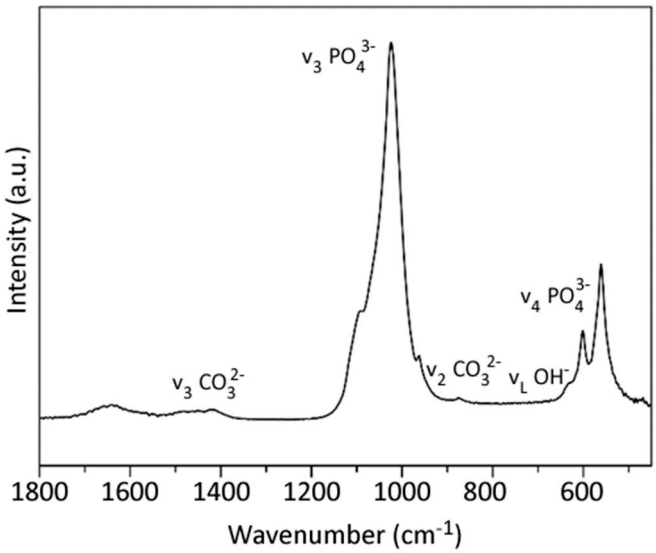

Figure 4. Fourier transform infrared (FT-IR) spectra of *n*HA in the region from 1800 cm^{-1} to 400 cm^{-1}.

3.2. Seed Germination and Root Elongation

The germination experiment was carried out to ascertain whether the exposure of the tomato seeds to increasing doses of CMC-*n*HA had any consequence on the germination process. Figures 5 and 6 report the percentage of germination and seedling root elongation, respectively.

While the germination percentage was not influenced by the increase in concentration of CMC-*n*HA (Figure 5), the root elongation of tomato seedlings was clearly affected. In fact, experimental data clearly demonstrated a dose-related stimulating effect promoted by 200–2000 mg L^{-1} CMC-*n*HA that was confirmed by ANOVA ($p < 0.001$). The root length increase compared to the control amounted to +64% and +97%, respectively, for 200 and 500 mg L^{-1} (Figure 6).

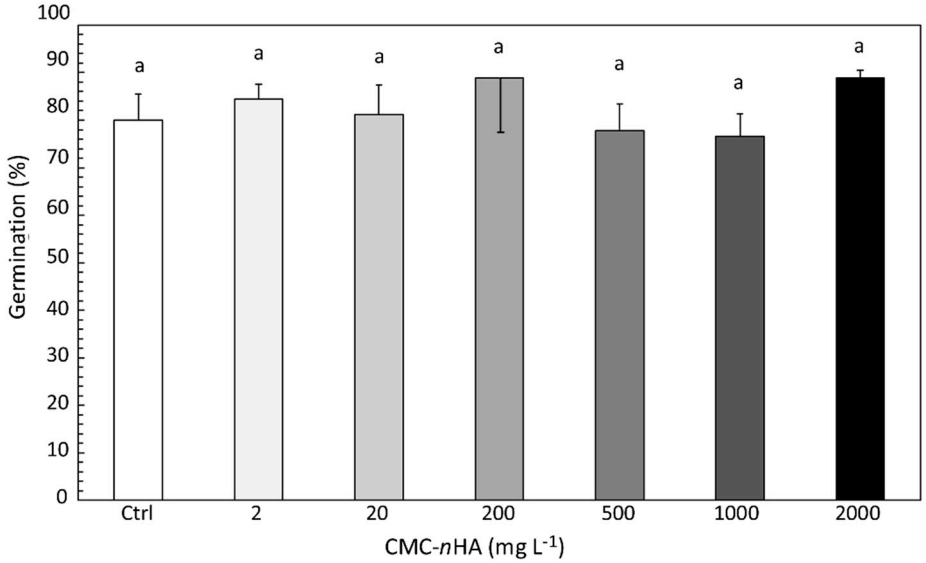

Figure 5. Effect of CMC-*n*HA on the percentage of germination of *S. lycopersicum*. Bars represent the mean standard deviation. Different letters indicate statistically significant differences between treatments (LSD test, $p \leq 0.05$).

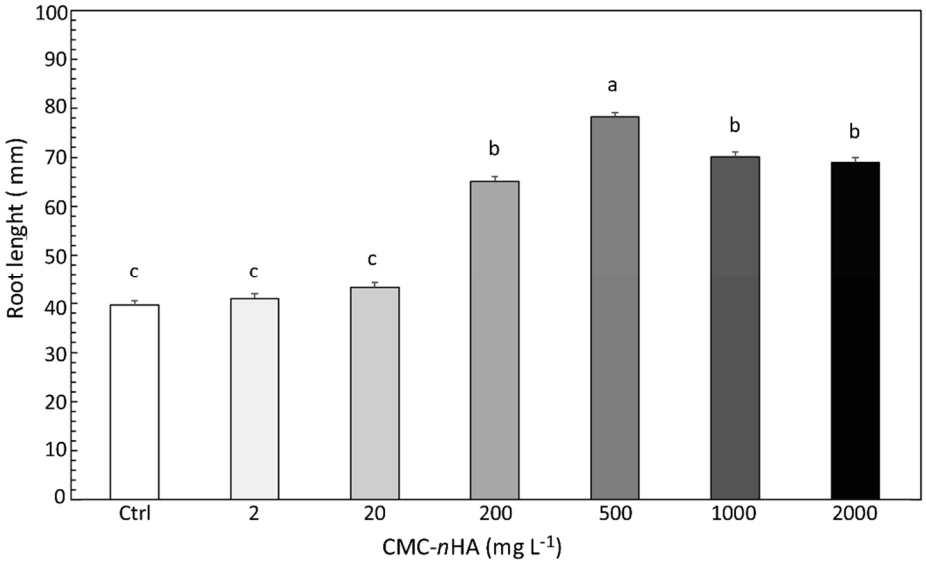

Figure 6. Effect of CMC-*n*HA on primary root elongation of *S. lycopersicum*. Bars represent the mean standard deviation. Different letters indicate statistically significant differences between treatments (LSD test, $p \leq 0.05$).

3.3. Plant Metabolism

Treatments with doses of CMC-*n*HA ranging from 20 and 2000 *n*HA were also tested to evaluate their effects on photosynthetic pigments (Table 2). In addition, the experimental plan was enriched with a treatment of bHA at 2000 mg L^{-1}. The quantification of pigments was carried out by spectrophotometric analysis of extracts obtained from plants subjected to different treatments for 48 h.

Table 2. One-way ANOVA analysis performed on photosynthetic pigments of *S. lycopersicum* seedlings to evaluate the effect of different concentrations of CMC-*n*HA and bHA.

Treatment	Chl a	Chl b	Carotenoids	Chl a/Chl b	Pheophytin
(mg L^{-1})	(μg g^{-1} FW)	(μg g^{-1} FW)	(μg g^{-1} FW)		(%)
0	475 ± 100 a	182 ± 47 ab	131 ± 21 a	3.18 ± 0.57 a	8.75 ± 0.93 ab
20	594 ± 174 a	193 ± 30 a	156 ± 47 a	3.03 ± 0.44 a	8.65 ± 0.34 b
200	466 ± 148 a	182 ± 18 ab	115 ± 39 a	2.66 ± 0.08 a	10.01 ± 0.87 a
500	430 ± 131 a	154 ± 38 ab	113 ± 34 a	2.69 ± 0.43 a	9.27 ± 1.22 ab
2000	451 ± 99 a	142 ± 11 b	121 ± 31 a	2.97 ± 0.18 a	9.11 ± 0.42 ab
2000 bHA	524 ± 127 a	161 ± 40 ab	140 ± 35 a	3.17 ± 0.16 a	9.04 ± 1.27 ab
F	0.883	1.576	0.952	1.155	1.118
p	0.509 ns	0.209 ns	0.468 ns	0.363 ns	0.382 ns

F = calculated *F* test value; *p* = statistical difference among average values; ns = not significant. Different letters indicate statistically significant differences between treatments (LSD test).

It was not possible to evidence any significant effect of the different treatments, except for a decrease of Chl b observed when the 2000 CMC-*n*HA treatment was applied. Pheophytin, a known metabolite associated to Photosystem II or involved in chlorophyll turnover, exhibited a bell-shaped profile, peaking at 200 mg L^{-1} dose of CMC-*n*HA. This value showed a significant difference compared to that measured at 20 mg L^{-1} nHA concentration.

The redox balance of seedling shoot and root portions was scarcely influenced by CMC-*n*HA treatments, as shown by ANOVA analysis (Table 3), where ROS were evaluated by means of the fluorescent probe H_2DCFDA.

Table 3. One-way ANOVA analysis performed on reactive oxygen species (ROS) and ATP content measured in S. lycopersicum seedlings to evaluate the effect of different concentrations of CMC-*n*HA and bHA.

Treatment	Root H_2DCFDA Fluorescence	Shoot H_2DCFDA Fluorescence	Root ATP	Shoot ATP
(mg L^{-1})	(A.U. mg^{-1} prot.)	(A.U. mg^{-1} prot.)	(nmol g^{-1} DW)	(nmol g^{-1} DW)
0	93 ± 27 a	57 ± 8 a	0.90 ± 0.23 a	28.87 ± 9.46 a
20	75 ± 27 a	50 ± 21 a	0.91 ± 0.03 a	28.37 ± 7.15 ab
200	78 ± 20 a	68 ± 15 a	0.75 ± 0.23 ab	25.66 ± 9.87 ab
500	61 ± 9 a	67 ± 14 a	0.76 ± 0.19 ab	18.18 ± 5.89 bc
2000	74 ± 17 a	68 ± 15 a	0.50 ± 0.12 b	14.27 ± 6.45 c
2000 bHA	83 ± 58 a	66 ± 14 a	0.68 ± 0.38 ab	31.08 ± 2.07 a
F	0.630	1.108	2.240	3.874
p	0.678 ns	0.384 ns	0.088 ns	0.013 *

F = calculated *F* test value; *p* = statistical difference among average values. *, $p < 0.05$; ns = not significant. Different letters indicate statistically significant differences between treatments (Least Significant Difference (LSD) test).

In the case of ATP content, in roots, a decreasing pattern in ATP content was inversely linked to increasing CMC-*n*HA concentrations, although a significant difference with respect to the control was appreciable only for the 2000 CMC-*n*HA dose. Noteworthy, at the same concentration, bHA did not induce any significant effect in both ROS and ATP concentrations. Consistently, also in the shoot the ANOVA of the overall CMC-*n*HA and bHA treatment showed a significant effect ($p < 0.05$). The doses at 500 and 2000 CMC-*n*HA mg L^{-1} strongly lowered the ATP amount with respect to the control.

3.4. P and Ca Content

The influence of the different CMC-*n*HA additions on P and Ca content in the shoot and root tissues was also analyzed by ICP-MS means (Figures 7 and 8). In particular, the analytic detection of P did not evidence any statistically significant differences in both plant fractions ($p = 0.07$).

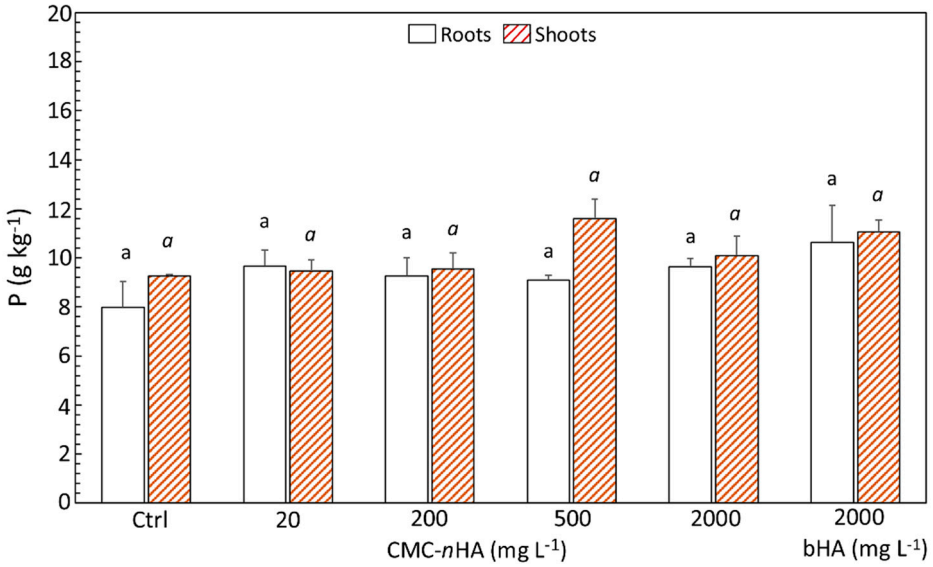

Figure 7. P concentration (g kg^{-1}) in the roots and shoots of *S. lycopersicum* seedlings. Bars represent the mean standard deviation. Different letters indicate statistically significant differences between treatments (Mann-Whitney (MWW) test, $p \leq 0.05$).

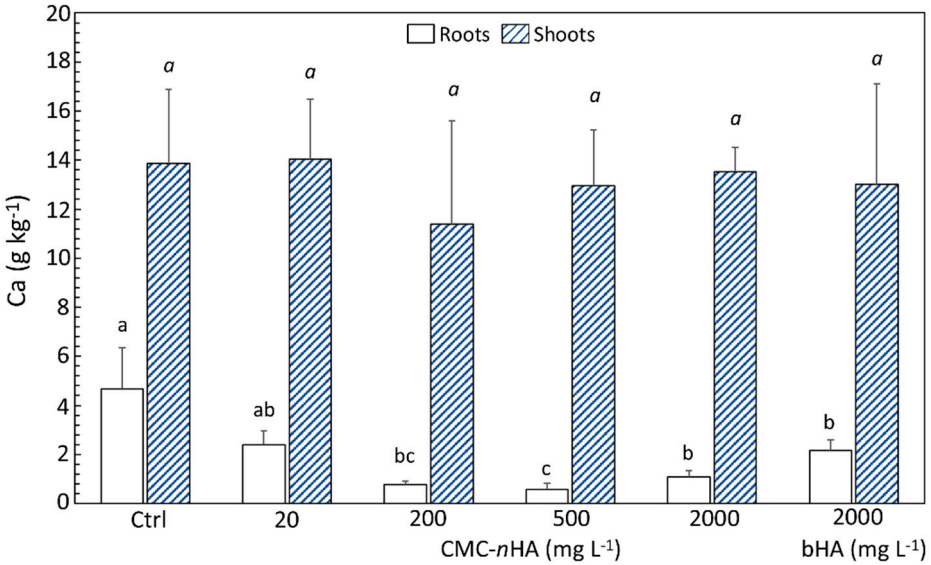

Figure 8. Ca concentration (g kg^{-1}) in the roots and shoots of *S. lycopersicum* seedlings. Bars represent the mean standard error. Different letters indicate statistically significant differences between treatments (MWW test, $p \leq 0.05$).

The results for the concentrations of P in roots were not significantly different between the control plants and the treated ones and among the treatments (Figure 7). However, the control plants had the lowest concentration of P in this portion (7.99 ± 2.32 g kg^{-1}) compared to the CMC-*n*HA treatments, while the highest concentration was measured in the roots of the plants treated with bHA (10.63 ± 3.39 g kg^{-1}).

The same statistical results were obtained for the concentrations of P in the shoot portions of the treated plants. Additionally, in this case, the control plants had the lowest concentration of P (9.25 ± 0.15 g kg^{-1}) compared to the other treatments, while the highest value was measured for the plants treated with CMC-*n*HA at 500 mg L^{-1} (11.60 ± 1.38 g kg^{-1}).

Regarding the Ca concentrations in the plant tissues, no significant differences were highlighted among the treatments in the shoot fractions. In fact, the concentrations of Ca had a comparable average value in all the treatments, the only exception was represented by the shoots of the plants treated with CMC-*n*HA at 200 (mg L^{-1}) that was slightly lower (11.40 ± 4.20 g kg^{-1}) when compared to the others (Figure 8). Instead, the MWW post-hoc analysis puts in evidence statistically significant differences among the treatments at root level ($p < 0.01$). Briefly, the control plants had the highest concentration of Ca among all treatments, that resulted as 4 times higher than the lowest one measured in the plants treated with *CMC-nHA* at 500 (mg L^{-1}). In general, the CMC-*n*HA treatments look likely to have an inhibitory effect on the uptake of Ca at the root level as their concentration increases. This trend remained constant in the plants treated with CMC-*n*HA up to the dose of 500 (mg L^{-1}). The concentrations of Ca returned to a slight increase from the CMC-*n*HA treatment at 2000 (mg L^{-1}) and this response was further enhanced when the treatment with bHA at 2000 (mg L^{-1}) was applied.

4. Discussion

The debate on the sustainability of the worldwide food system has recently received a renewed boost due to the report published in early 2019 by the EAT-Lancet Commission [26]. The report stated that "the current global food system requires a new agricultural revolution that is based on sustainable intensification and driven by sustainability and system innovation". In connection with this, the rapid development of knowledge on the application of nanotechnology in agriculture will have to provide the necessary innovation to produce a significant leap forward in the efficiency of agricultural crop fertilization techniques.

As previously mentioned, nanofertilizer application has an edge over conventional fertilizer application due to the controlled release of nutrients, preventing groundwater pollution and eutrophication in freshwater and coastal marine ecosystems [27,28]. The NUE increase also translates into a decrease of fertilizers used, which means a reduction in production costs. However, the deliberate introduction of nanomaterials in agriculture raises questions and expresses concerns over the possible human and environmental health implications.

Early nano-ecotoxicological studies evidenced that nanomaterials could have toxic effect not only on plants, but also on various soil microorganisms including yeasts, bacteria, and fungi [29]. In this perspective, the purpose of achieving sustainable agriculture overlaps the need of balancing the benefits provided by nano-products in solving environmental challenges with the assessment and management of environmental, health, and safety risks potentially created by nanoscale materials [30]. Since nanomaterials or nano-products are intended to neither affect human health nor alter the environment along their life cycle, engineered nanomaterials (ENMs) design and safety assessment should be integrated. The approach will foster nanomaterials safer-by-design by considering both applications and implications [31]. This implies that the behavior of nanomaterials should be thoroughly investigated before their release.

The purpose of our study was to undertake preliminary observation regarding the possible use of *n*HA in plant nutrition, both as a direct source of P and Ca and as a carrier for other nutrients.

The characterization of the *n*HA employed within this study was already reported in [32,33]. *n*HA have the typical characteristics of biological hydroxyapatites, such as nanometric dimension, poor crystallinity and non-stoichiometric composition. In this work, *n*HA were suspended in a Hoagland solution and CMC in order to obtain stable colloidal suspensions of nanoparticles to be used on tomato plants. The so obtained colloidal suspensions were stable up to the highest concentration and for the time required for the experiments on plants (i.e., 2000 mg mL^{-1} up to 48 h), as demonstrated by the direct comparison reported in Figure 3 of the Hd size distributions recorded at 30 min and 48 h after their obtainment.

The influence of ENMs—whether they are metallic or carbon-based materials—on plants was discussed in recent reviews [34–37]. Since most of these studies have been conducted in the laboratory or under controlled conditions, seed germination and seedling growth are among the most studied stages of plant development. While taking into account that a generalization could be premature due to the variety of factors involved (plant species, type, and properties of ENMs and concentrations), it seems that ENMs in low or not-extreme doses are capable of stimulating seed germination, seedling growth, and root development in different plant species [38–40].

As regards the enhancement of germination, the physiological basis of such a response are still to be clarified; however, it is possibly related to a physical interaction between ENMs and the seed structure, which makes the water uptake by the germinating seed more efficient. Then, it is conceivable that a higher absorption of water and nutrients may correspond to an increase in translocation and a corresponding increase in the aerial biomass of the plant. Studies conducted on tomatoes treated with metal nanoparticles demonstrated positive effects on germination induced by *n*SiO_2 [41] and no effects in seeds treated with *n*TiO_2 [42,43]. In parallel, there were observed also negative effects on seed germination and root elongation, respectively, in the cases of *n*CeO_2 [43] and *n*ZnO [44].

Germinating seeds and seedlings of tomatoes were treated also with C-based nanomaterials. In this case, enhanced germination percentage and seedling growth in response to treatments with single walled carbon nanotubes [45,46] and multiple walled carbon nanotubes [47,48] were observed. Tomato seedlings treated with different concentrations of graphene developed longer roots, but with a lower biomass accumulation than the control [49].

Specific observations regarding the influence of *n*HA on seed germination and seedling growth have been reported, as far as we know, in a single paper [16]. Actually, that study compared the effects of the nanohybrid Urea-*n*HA and Urea alone on seed germination and seedling growth of *Vigna radiata*, respectively. In both cases, the nanohybrid gave the better results, increasing the germination rate

and the biomass yield of *V. radiata*. In our experiment, was used a different nanomaterial than in the abovementioned studies and therefore we are not able to confirm or contrast such results. However, under the conditions of our experiment the germination of tomato seeds was indifferent to the increase in concentration of CMC-*n*HA.

On the other hand, we observed a positive response of root elongation to the increase in CMC-*n*HA concentration. In connection with this, it is advisable to make two considerations. Firstly, according to Rouached et al. 2010 [50], plant root development is the major plant growth parameter associated with abiotic stress or toxic agents. Secondly, bioavailable P is the major element limiting the growth and yield of crops [51]. Therefore, increasing the concentration of CMC-nHA we did not observe toxic effects on tomato seedlings. Furthermore, increased readily available fraction of P stimulated root elongation, which is the necessary condition for plant growth [52].

This result also confirms the well-known reduction on primary root growth observed in plants subjected to low phosphate availability, as described in *Arabidopsis* [53]. We will be able to confirm this hypothesis by conducting a longer experiment observing the plant growth rate and fraction biomass yield.

Regarding the photosynthetic pigments measured in tomato plantlets grown in hydroponic culture, the collected data revealed that the addition of CMC-*n*HA to different concentrations was substantially ineffective. Only the 2000 mg L^{-1} dose could display some anomalous outcome as in the case of photosynthetic pigments. The chlorophyll b was partially affected by the highest CMC-*n*HA treatment and this could be explained as a partial increase of chlorophyll degradation. Noteworthy, the bHA treatment given at the same dose was not able to induce any modification, so the physical form of the HA was crucial. In addition, pheophytin content also exhibited a peak corresponding to the 200 mg L^{-1} dose. Although the ANOVA analysis did not show any significance for the overall treatment, the peak could represent a rearrangement of the photosynthetic machinery, possibly by chlorophyll recycling and increase of the Photosystem II presence.

The measurement of ATP in different plant portions was chosen as a proof of bio-energetic equilibrium in the treated plantlets. In the roots, only the 2000 mg L^{-1} dose was able to decrease the nucleotide concentration, but in the case of the autotrophic shoots, the decline of the ATP was sharp and this is the only parameter that exhibited a significant effect after ANOVA analysis (p = 0.013). The alteration of this metabolic indicator was restricted mainly to the aerial plant fraction, where ATP content is one order magnitude higher than in roots, and it could be tentatively explained in terms of signaling unbalance and photosynthesis impairment. Actually, in the autotrophic portion of the shoot, the contribution to energy balance is mainly due to photosynthesis that seemed to be more sensitive when the treatments largely exceeded the usual need. In fact, the addition of high concentration *n*HA has a negative impact on ATP production probably because the high salinity induces stomata closure and consequently the photorespiration metabolism [54,55]. Such an event is energy demanding and is known to lower the ATP and NADPH content of the green tissues [56].

Regarding the amount of nutrients accumulated within the two distinct portions of the plant, P showed a marked difference in uptake with respect to Ca. Generally, P exhibits a more diffuse absorption area and a greater mobility inside the organ [57] and we suggest that, thanks to its more efficient uploading and transport inside the seedling, the content of P in the different tomato tissues was not affected by different CMC-*n*HA concentrations, even if compared to bHA treatment. Accordingly, the profile between the hypogeal and epigeal portion showed a similar trend (Figure 7).

On the contrary, Ca absorption and translocation was largely localized at new root hairs or at root tips [58]. In addition, a continuous removal of Ca from roots and subsequent transfer to epigeal organs occurred, without recirculation via phloem, as happens for other nutrients [59]. This unidirectional transport of Ca via xylem is a well-known phenomenon [60] and caused Ca accumulation in the stem with an order of magnitude higher when compared to the root (Figure 8). This process could have also masked the effects in the shoots induced by different doses of CMC-*n*HA, whereas a hormetic effect

induced by the different treatments was detectable in the root, this organ not being the main storage site for plant Ca pools.

High external calcium provoked a decrease in the internal concentration [61]. At root level, since Ca concentration and compartmentalization was finely tuned, the excess of nutrient progressively decreased the cell permeability and caused a decrease in the Ca loaded in the symplast [62]. The phenomenon was regulated by Ca^{2+}-channels mediated flux, which was driven by the concentration gradient [58], while the activity of the Ca-ATPase pumps counteracted Ca entry by partitioning inside storage organelles (vacuole, endoplasmic reticulum, and mitochondria) or in the apoplast [63]. At the equilibrium, the cytosolic content of Ca was buffered at nanomolar levels. By further increasing the external Ca gradient, the action of the Ca^{2+}-ATPase pumps was endangered by the growing demand for ATP, which was probably not adequately supported by respiration. In fact, the seedlings grew in hydroponic conditions, where a partial hypoxia stress definitely caused a decrease in respiratory efficiency. These factors could have been the basis for the low, but significant increase in Ca found at the highest doses of CMC-*n*HA [63,64]. This observation is substantiated by results about oxidative stress obtained with the same treatments. The evidence showed a decline in ROS, one of the events caused by reducing conditions and by the calcium-stimulation of antioxidant systems [65].

5. Conclusions

There is general agreement on the potential of nanotechnologies applied to the primary sector, and in particular on the declination of these towards sustainability. The deliberate introduction of nanomaterials within agricultural activities and in soil raises questions and concerns over the possible human and environmental health implications. In this perspective, the purpose of achieving sustainable agriculture overlaps the need of balancing the benefits provided by nano-products in solving environmental challenges with the assessment and management of environmental, health, and safety risks potentially posed by nanoscale materials.

This paper demonstrated that CMC-*n*HA—excluding at very high concentrations—had nontoxic effects on our model plant and therefore it could be used both as a P supplier and carrier of other elements and molecules. Our study will develop in this direction.

Author Contributions: M.I., A.A., E.B. and L.M. conceived and designed the experiments; M.I., A.A. and L.D.E. chemical analysis and *n*HA characterization; E.B., A.M. Writing—draft paper, editing and review, M.I., A.A., L.D.E., E.P., A.M., A.F., E.B. and L.M.; All authors read and approved the final manuscript.

Funding: This research work was funded by the Regione Friuli Venezia Giulia, project "Nanomateriali 2017–2020".

Acknowledgments: L.M. is grateful to Regione Friuli Venezia Giulia, General Directorate of Environment, for its financial support to the project "Nanomateriali 2017–2020". A.A. and M.I. thank the Elsevier Green and Sustainable Chemistry Foundation for providing financial support to the project "phos-FATE: Empowering fishing communities for climate change".

Conflicts of Interest: The authors declare no conflict of interest.

References

1. Pisante, M.; Stagnari, F.; Grant, C.A. Agricultural innovations for sustainable crop production intensification. *Ital. J. Agron.* **2012**, *7*, 40. [CrossRef]
2. López-Arredondo, D.L.; Sánchez-Calderón, L.; Yong-Villalobos, L. Molecular and genetic basis of plant macronutrient use efficiency: Concepts, opportunities and challenges. In *Plant Macronutrient Use Efficiency Molecular and Genomic Perspectives in Crop Plants*; Hossain, M.A., Kamiya, T., Burritt, D.Y., Phan Tran, L.-S., Fujiwara, T., Eds.; Academic Press: Cambridge, MA, USA, 2017; pp. 1–29. ISBN 978-0-12-811308-0.
3. Baligar, V.C.; Fageria, N.K. Nutrient use efficiency in plants: An overview. In *Nutrient Use Efficiency: From Basics to Advances*; Rakshit, A., Singh, H.B., Sen, A., Eds.; Springer: New Delhi, India, 2015; pp. 1–14. ISBN 978-81-322-2168-5.
4. Liu, R.; Lal, R. Potentials of engineered nanoparticles as fertilizers for increasing agronomic productions. *Sci. Total Environ.* **2015**, *514*, 131–139. [CrossRef]

5. Wang, P.; Lombi, E.; Zhao, F.-J.; Kopittke, P.M. Nanotechnology: A new opportunity in plant sciences. *Trends Plant Sci.* **2016**, *21*, 699–712. [CrossRef]
6. Duhan, J.S.; Kumar, R.; Kumar, N.; Kaur, P.; Nehra, K.; Duhan, S. Nanotechnology: The new perspective in precision agriculture. *Biotechnol. Rep.* **2017**, *125*, 11–23. [CrossRef]
7. Raliya, R.; Saharan, V.; Dimkpa, C.; Biswas, P. Nanofertilizer for precision and sustainable agriculture: Current state and future perspectives. *J. Agric. Food Chem.* **2018**, *66*, 6487–6503. [CrossRef]
8. Gogos, A.; Knauer, K.; Bucheli, T.D. Nanomaterials in plant protection and fertilization: Current state, foreseen applications, and research priorities. *J. Agric. Food Chem.* **2012**, *60*, 9781–9792. [CrossRef] [PubMed]
9. Kah, M.; Kookana, R.S.; Gogos, A.; Bucheli, T.D. A critical evaluation of nanopesticides and nanofertilizers against their conventional analogues. *Nat. Nanotechnol.* **2018**, *13*, 677–684. [CrossRef]
10. Dimkpa, C.O.; Bindraban, P.S. Nanofertilizers: New products for the industry? *J. Agric. Food Chem.* **2018**, *66*, 6462–6473. [CrossRef] [PubMed]
11. Calabi-Floody, M.; Medina, J.; Rumpel, C.; Condron, L.M.; Hernandez, M.; Dumont, M.; de la Luz Mora, M. Smart fertilizers as a strategy for sustainable agriculture. *Adv. Agron.* **2018**, *147*, 119–157. [CrossRef]
12. Gómez-Morales, J.; Iafisco, M.; Delgado López, J.M.; Stéphanie, S.; Drouet, C. Progress on the preparation of nanocrystalline apatites and surface characterization: Overview of fundamental and applied aspects. *Prog. Cryst. Growth Charact. Mater.* **2013**, *59*, 1–46. [CrossRef]
13. Tampieri, A.; Iafisco, M.; Sprio, S.; Ruffini, A.; Panseri, S.; Montesi, M.; Adamiano, A.; Sandri, M. Hydroxyapatite: From Nanocrystals to Hybrid Nanocomposites for Regenerative Medicine. In *Handbook of Bioceramics and Biocomposites*; Antoniac, I., Ed.; Springer: Cham, Switzerland, 2016; pp. 119–144. [CrossRef]
14. Sprio, S.; Sandri, M.; Ruffini, A.; Adamiano, A.; Iafisco, M.; Dapporto, M.; Panseri, S.; Montesi, M.; Tampieri, A. Tissue Engineering and Biomimetics with Bioceramics. In *Advances in Ceramic Biomaterials*; Palmero, P., Cambier, F., De Barra, E., Eds.; Woodhead Publishing: Cambridge, UK, 2017; pp. 407–432. [CrossRef]
15. Kottegoda, N.; Munaweera, I.; Madusanka, N.; Karunaratne, V. A green slow-release fertilizer composition based on urea-modified hydroxyapatite nanoparticles encapsulated wood. *Curr. Sci.* **2011**, *101*, 73–78.
16. Subbaiya, R.; Priyanka, M.; Masilamani Selvam, M. Formulation of green nano-fertilizer to enhance the plant growth through slow and sustained release of nitrogen. *J. Pharm. Res.* **2012**, *5*, 5178–5183.
17. Kottegoda, N.; Sandaruwan, C.; Priyadarshana, G.; Siriwardhana, A.; Rathnayake, U.A.; Berugoda Arachchige, D.M.; Kumarasinghe, A.R.; Dahanayake, D.; Karunaratne, V.; Amaratunga, G.A.J. Urea-hydroxyapatite nanohybrids for slow release of nitrogen. *ACS Nano* **2017**, *11*, 1214–1221. [CrossRef]
18. Gunaratne, G.P.; Kottegoda, N.; Madusanka, N.; Munaweera, I.; Sandaruwan, C.; Priyadarshana, W.M.G.I.; Siriwardhana, A.; Madhushanka, B.A.D.; Rathnayake, U.A.; Karunaratne, V. Two new plant nutrient nanocomposites based on urea coated hydroxyapatite: Efficacy and plant uptake. *Indian J. Agric. Sci.* **2016**, *86*, 494–499.
19. Madusanka, N.; Sandaruwana, C.; Kottegoda, N.; Sirisena, D.; Munaweera, I.; De Alwis, A.; Karunaratnea, V.; Amaratunga, G.A.J. Urea–hydroxyapatite-montmorillonite nanohybrid composites as slow release nitrogen compositions. *Appl. Clay Sci.* **2017**, *150*, 303–308. [CrossRef]
20. Liu, R.; Lal, R. Synthetic apatite nanoparticles as a phosphorus fertilizer for soybean (*Glycine max*). *Sci. Rep.* **2014**, *4*, 5686–5691. [CrossRef]
21. Montalvo, D.; McLaughlin, M.J.; Degryse, F. Efficacy of hydroxyapatite nanoparticles as phosphorus fertilizer in andisols and oxisols. *Soil Sci. Soc. Am. J.* **2015**, *79*, 551–558. [CrossRef]
22. Sandhöfer, B.; Meckel, M.; Delgado-López, J.M.; Patrício, T.; Tampieri, A.; Rösch, F.; Iafisco, M. Synthesis and preliminary in vivo evaluation of well-dispersed biomimetic nanocrystalline apatites labeled with positron emission tomographic imaging agents. *ACS Appl. Mater. Interfaces* **2015**, *19*, 10623–10633. [CrossRef]
23. Filippi, A.; Zancani, M.; Petrussa, E.; Braidot, E. Caspase-3-like activity and proteasome degradation in grapevine suspension cell cultures undergoing silver-induced programmed cell death. *J. Plant Physiol.* **2018**, *233*, 42–51. [CrossRef]
24. Mobin, M.; Khan, N.A. Photosynthetic activity, pigment composition and antioxidative response of two mustard (*Brassica juncea*) cultivars differing in photosynthetic capacity subjected to cadmium stress. *J. Plant Physiol.* **2007**, *164*, 601–610. [CrossRef]

25. Mattiello, A.; Pošćić, F.; Musetti, R.; Giordano, C.; Vischi, M.; Filippi, A.; Bertolini, A.; Marchiol, L. Evidences of genotoxicity and phytotoxicity in *Hordeum vulgare* exposed to CeO_2 and TiO_2 nanoparticles. *Front. Plant Sci.* **2015**, *6*, 1043. [CrossRef]
26. Willett, W.; Rockström, J.; Loken, B.; Springmann, M.; Lang, T.; Vermeulen, S.; Garnett, T.; Tilman, D.; DeClerck, F.; Wood, A.; et al. Food in the Anthropocene: The EAT–Lancet Commission on healthy diets from sustainable food systems. *Lancet* **2019**. [CrossRef]
27. Naderi, M.R.; Danesh-Shahraki, A. Nanofertilizers and their roles in sustainable agriculture. *Int. J. Agric. Crop Sci.* **2013**, *5*, 2229–2232.
28. Sekhon, B.S. Nanotechnology in agri-food production: An overview. *Nanotechnol. Sci. Appl.* **2014**, *7*, 31–53. [CrossRef]
29. Rajput, V.D.; Minkina, T.; Sushkova, S.; Tsitsuashvili, V.; Mandzhieva, S.; Gorovtsov, A.; Nevidomskyaya, D.; Gromakova, N. Effect of nanoparticles on crops and soil microbial communities. *J. Soils Sedim.* **2018**, *18*, 2179–2187. [CrossRef]
30. Iavicoli, I.; Leso, V.; Beezhold, D.H.; Shvedova, A.A. Nanotechnology in agriculture: Opportunities, toxicological implications, and occupational risks. *Toxicol. Appl. Pharm.* **2017**, *329*, 96–111. [CrossRef]
31. Lin, S.; Yu, T.; Yu, Z.; Hu, X.; Yin, D. Nanomaterials Safer-by-Design: An Environmental Safety Perspective. *Adv. Mater.* **2018**, 1705691. [CrossRef]
32. Iafisco, M.; Bosco, R.; Leeuwenburgh, S.C.; van den Beucken, J.J.J.P.; Jansen, J.A.; Prat, M.; Roveri, N. Electrostatic spray deposition of biomimetic nanocrystalline apatite coatings onto titanium. *Adv. Eng. Mater.* **2012**, *14*, B13–B20. [CrossRef]
33. Bosco, R.; Iafisco, M.; Tampieri, A.; Jansen, J.A.; Leeuwenburgh, S.C.; Van Den Beucken, J.J. Hydroxyapatite nanocrystals functionalized with alendronate as bioactive components for bone implant coatings to decrease osteoclastic activity. *Appl. Surf. Sci.* **2015**, *328*, 516–524. [CrossRef]
34. Husen, A.; Siddiqi, K.S. Carbon and fullerene nanomaterials in plant system. *J. Nanobiotechnol.* **2014**, *12*. [CrossRef]
35. Vithanage, M.; Seneviratne, M.; Ahmad, M.; Sarkar, B.; Ok, Y.S. Contrasting effects of engineered carbon nanotubes on plants: A review. *Environ. Geochem. Health* **2017**, *39*, 1421–1439. [CrossRef]
36. Dimkpa, C.O. Soil properties influence the response of terrestrial plants to metallic nanoparticles exposure. *Curr. Opin. Environ. Sci. Health* **2018**, *6*, 1–8. [CrossRef]
37. Pandey, K.; Lahiani, M.H.; Hicks, V.K.; Hudson, M.K.; Green, M.J.; Khodakovskaya, M. Effects of carbon-based nanomaterials on seed germination, biomass accumulation and salt stress response of bioenergy crops. *PLoS ONE* **2018**, *13*, e0202274. [CrossRef]
38. Rico, C.M.; Majumdar, S.; Duarte-Gardea, M.; Peralta-Videa, J.R.; Gardea-Torresdey, J.L. Interaction of nanoparticles with edible plants and their possible implications in the food chain. *J. Agric. Food Chem.* **2011**, *59*, 3485–3498. [CrossRef]
39. Miralles, P.; Church, T.L.; Harris, A.T. Toxicity, uptake, and translocation of engineered nanomaterials in vascular plants. *Environ. Sci. Technol.* **2012**, *46*, 9224–9239. [CrossRef]
40. Lahiani, M.H.; Dervishi, E.; Ivanov, I.; Chen, J.; Khodakovskaya, M. Comparative study of plant responses to carbon-based nanomaterials with different morphologies. *Nanotechnology* **2016**, *27*, 265102. [CrossRef]
41. Siddiqui, M.H.; Al-Whaibi, M.H. Role of nano-SiO_2 in germination of tomato (*Lycopersicum esculentum*) seeds mill. *Saudi J. Biol. Sci.* **2014**, *21*, 13–17. [CrossRef]
42. Raliya, R.; Biswasa, P.; Tarafdarm, J.C. TiO_2 nanoparticle biosynthesis and its physiological effect on mung bean (*Vigna radiata* L.). *Biotechnol. Rep.* **2015**, *5*, 22–26. [CrossRef]
43. Andersen, C.P.; King, G.; Plocher, M.; Storm, M.; Pokhrel, L.R.; Johnson, M.G.; Rygiewicz, P.T. Germination and early plant development of ten plant species exposed to titanium dioxide and cerium oxide nanoparticles. *Environ. Toxicol. Chem.* **2016**, *35*, 2223–2229. [CrossRef]
44. De la Rosa, G.; López-Moreno, M.L.; de Haro, D.; Botez, C.E.; Peralta-Videa, J.R.; Gardea-Torresdey, J.L. Effects of ZnO nanoparticles in alfalfa, tomato, and cucumber at the germination stage: Root development and X-ray absorption spectroscopy studies. *Pure Appl. Chem.* **2013**, *85*, 2161–2174. [CrossRef]
45. Khodakovskaya, M.V.; de Silva, K.; Nedosekin, D.A.; Dervishi, E.; Biris, A.S.; Shashkov, E.V.; Galanzha, E.I.; Zharov, V.P. Complex genetic, photothermal, and photoacoustic analysis of nanoparticle-plant interactions. *Proc. Natl. Acad. Sci. USA* **2011**, *108*, 1028–1033. [CrossRef]

46. Haghighi, M.; Teixeira da Silva, J.A. The effect of carbon nanotubes on the seed germination and seedling growth of four vegetable species. *J. Crop Sci. Biotechnol.* **2014**, *17*, 201–208. [CrossRef]
47. Morla, S.; Rao, C.R.; Chakrapani, R. Factors affecting seed germination and seedling growth of tomato plants cultured in vitro conditions. *J. Chem. Biol. Phys. Sci.* **2011**, *1*, 328–334.
48. Tiwari, D.K.; Dasgupta-Schubert, N.; Villasenor, L.M.; Tripathi, D.; Villegas, J. Interaction of carbon nanotubes with mineral nutrients for the promotion of growth of tomato seedlings. *Nano Stud.* **2013**, *7*, 87–96.
49. Zhang, M.; Gao, B.; Chen, J.; Li, Y.; Zhang, M.; Gao, B.; Chen, J.; Li, Y. Effects of graphene on seed germination and seedling growth. *J. Nanoparticle Res.* **2015**, *17*, 78. [CrossRef]
50. Rouached, H.; Bulak Arpat, B.; Poirier, Y. Regulation of phosphate starvation responses in plants: Signaling players and cross-talks. *Mol. Plant* **2010**, *3*, 288–299. [CrossRef]
51. Ogawa, S.; Gomez Selvaraj, M.; Fernando, A.J.; Lorieux, M.; Ishitani, M.; McCouch, S.; Arbelaez, J.D. N- and P-mediated seminal root elongation response in rice seedlings. *Plant Soil* **2014**, *375*, 303–315. [CrossRef]
52. Bengough, A.G.; McKenzie, B.M.; Hallett, P.D.; Valentine, T.A. Root elongation, water stress, and mechanical impedance: A review of limiting stresses and beneficial root tip traits. *J. Exp. Bot.* **2011**, *62*, 59–68. [CrossRef]
53. Williamson, L.C.; Ribrioux, S.P.C.P.; Fitter, A.H.; Ottoline Leyser, H.M. Phosphate availability regulates root system architecture in *Arabidopsis*. *Plant Physiol.* **2001**, *126*, 875–882. [CrossRef]
54. De Silva, D.L.R.; Hetherington, A.M.; Mansfield, T.A. Where does all the calcium go? Evidence of an important regulatory role for trichomes in two calcicoles. *Plant Cell Environ.* **1996**, *19*, 880–886. [CrossRef]
55. Tanner, W.; Beevers, H. Transpiration, a prerequisite for long distance transport of minerals in plants? *Proc. Natl. Acad. Sci. USA* **2001**, *98*, 9443–9447. [CrossRef]
56. Heber, U.; Krause, G.H. What is the physiological role of photorespiration. *Trends Biochem. Sci.* **1980**, *5*, 32–34. [CrossRef]
57. Kirkby, E.A.; Pilbeam, D.J. Calcium as a plant nutrient. *Plant Cell Environ.* **1984**, *7*, 397–405. [CrossRef]
58. White, P.J.; Broadley, M.R. Calcium in plants. *Ann. Bot.* **2003**, *92*, 487–511. [CrossRef]
59. Conn, S.; Gilliham, M. Comparative physiology of elemental distributions in plants. *Ann Bot.* **2010**, *105*, 1081–1102. [CrossRef]
60. Dayod, M.; Tyerman, S.D.; Leigh, R.A.; Gilliham, M. Calcium storage in plants and the implications for calcium biofortification. *Protoplasma* **2010**, *247*, 215–231. [CrossRef]
61. Hepler, P.H. Calcium: A Central Regulator of Plant Growth and Development. *Plant Cell* **2005**, *17*, 2142–2155. [CrossRef]
62. Miedema, H.; Bothwell, J.H.; Brownlee, C.; Davies, J.M. Calcium uptake by plant cells -channels and pumps acting in concert. *Trends Plant Sci.* **2001**, *6*, 514–519. [CrossRef]
63. Igamberdiev, A.U.; Hill, R.D. Elevation of cytosolic Ca2+ in response to energy deficiency in plants: The general mechanism of adaptation to low oxygen stress. *Biochem. J.* **2018**, *475*, 1411–1425. [CrossRef]
64. Igamberdiev, A.U.; Kleczkowski, L.A. Magnesium and cell energetics in plants under anoxia. *Biochem. J.* **2011**, *437*, 373–379. [CrossRef]
65. He, L.; Li, B.; Lu, X.; Yuan, L.; Yang, Y.; Yuan, Y.; Du, J.; Guo, S. The effect of exogenous calcium on mitochondria, respiratory metabolism enzymes and ion transport in cucumber roots under hypoxia. *Sci. Rep.* **2015**, *5*, 11391. [CrossRef]